Supporting Information

X-Ray Photoelectron Spectroscopic and Resonant X-Ray Spectroscopic Investigations of Interactions Between Thin Metal Catalyst Films and Amorphous Titanium Dioxide Photoelectrode Protection Layers

Matthias H. Richter‡, Wen-Hui Cheng‡, Ethan J. Crumlin, Walter S. Drisdell,

Harry A. Atwater, Dieter Schmeißer, Nathan S. Lewis*, and Bruce S. Brunschwig*

* Correspondence to: nslewis@caltech.edu, bsb@caltech.edu

‡ These authors contributed equally to the work.

The PDF file includes:

Figure S1 to S12

Equation S1 to S5

Table S1

References 1 to 8

Resonant Photoemission

Standard X-Ray photoelectron spectroscopy involves the measurement of core level (CL, Figure S1, process I) and valence band (VB) states (Figure S1, process II) of a sample. Due to the characteristic binding energies ($\boldsymbol{E}_B$) for core level excitations, different element and oxidations states can be usually identified without difficulty. However, for VB spectroscopy all elements have their electronic states within a few eV of the Fermi energy ($\boldsymbol{E}_F$), making their transitions overlap. Resonant excitation of core levels enables observation of the VB states associated with a particular element. With Ti as an example, these processes are described by Equation S1-S5. Equation S1 and Equation S2 describe normal XPS excitations of Ti 2p core and VB levels. In these transitions the excitation energy $\hbar\omega''$ is fixed.

$$\text{Ti } 2p^6 + \hbar\omega'' \rightarrow \text{Ti } 2p^5 + e_{vac}^- \quad \text{(Equation S1)}$$

$$[VB]^n + \hbar\omega'' \rightarrow [VB]^{n-1} + e_{vac}^- \quad \text{(Equation S2)}$$

$$\text{Ti } 2p^6 + [VB]^n + [CB]^0 + \hbar\omega \rightarrow \text{Ti } 2p^5 + [VB]^n + [CB]^1 \quad \text{(Equation S3)}$$

$$\text{Ti } 2p^5 + [VB]^n + [CB]^1 \rightarrow \text{Ti } 2p^6 + [VB]^{n-1} + [CB]^0 + e_{vac}^- \quad \text{(Equation S4)}$$

$$\text{Ti } 2p^5 + [VB]^n + [CB]^1 \rightarrow \text{Ti } 2p^6 + [VB]^{n-1} + [CB]^1 + \hbar\omega' \quad \text{(Equation S5)}$$

For tunable excitation sources, the energy is chosen to excite a core level electron into a bound empty state of the conduction band, as shown in Equation S3. The resonant excitation is governed by dipole selection rules. [1] The excitation is normally element-specific and transition-specific. The resonantly excited state in Equation S3 can relax into different final states by refilling the initially formed core hole by an electron. In our case, the refilling of the core hole by a valence electron results in two possible processes, in which a) the energy is transferred to the initial excited electron (Equation S4, participator Auger decay) or b) emitted as an X-Ray photon with a

characteristic energy. The same final state is reached in Equation S2 and Equation S4. Equation S3 and Equation S4 describe one channel of the observed resPES and eqn. Equation S3 and Equation S5 describe the RiXS process. The excitation in Equation S3 is element specific so the resPES yields the VB spectrum from a single elemental species.

The observed resPES must be corrected by subtracting the off-resonant VB spectrum as a background from the on-resonant excitation. Consequently, the VB spectrum from a single elemental species can be obtained. The background subtraction is not required for RiXS (Equation S5) because the emitted photons have a characteristic energy $\hbar\omega'$ for each element.

During resPES or RiXS experiments, the photon energy is scanned across the absorption edge of the element (Ti $L_{3/2}$ edge for excitation from Ti 2p core levels) of interest. At each photon energy, the emitted electron or X-Ray emissions, respectively, are collected and analyzed. The resPES or RiXS data are three-dimensional data sets of the signal intensity as a function of the excitation energy and either emitted the electron energy or X-Ray energy. Traditionally the binding energy is used in resPES whereas in RiXS spectra the loss energy ($\boldsymbol{E}_{\mathrm{loss}} = \hbar\omega - \hbar\omega'$) is used.

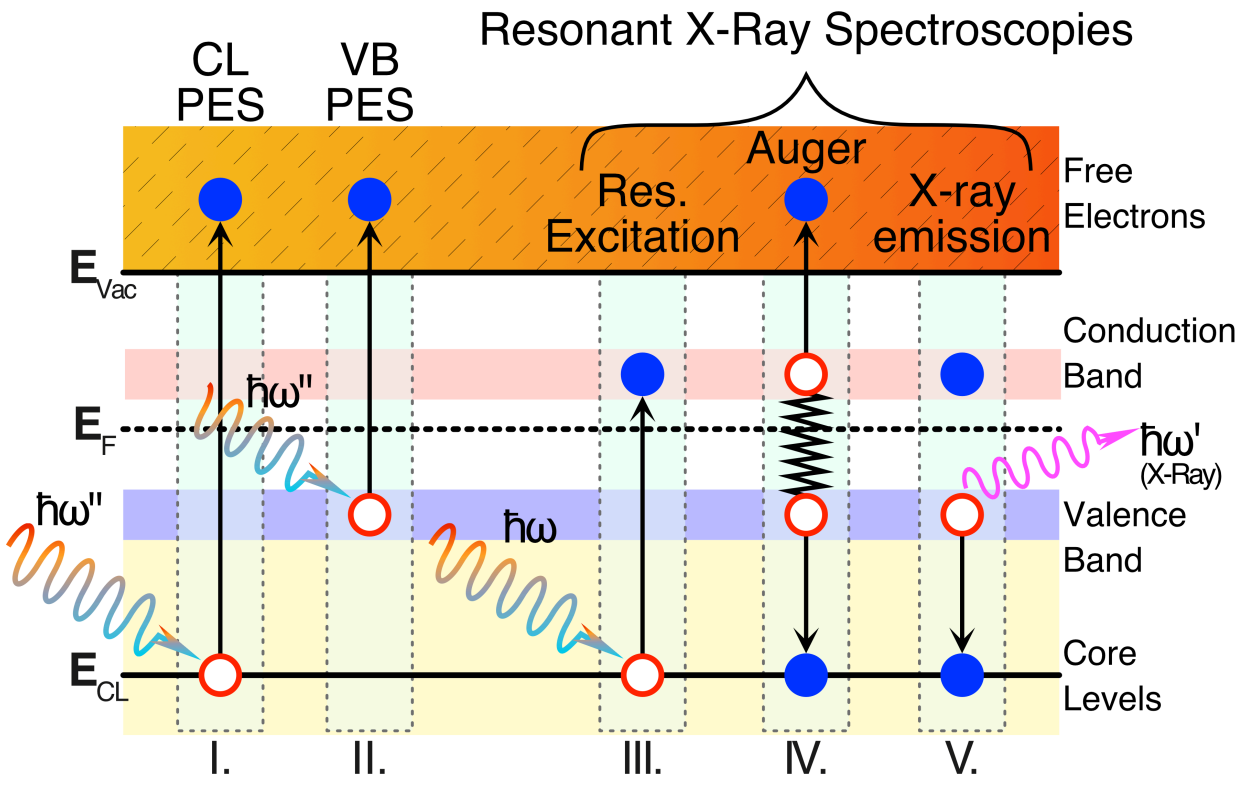

Figure S1: *Illustration of possible X-Ray spectroscopy excitation and decay channels:*

*I. Excitation of core level electron above the vacuum level (**E**$_{Vac}$, Equation S1);*

II. Excitation of VB electron above the vacuum level (Equation S2);

III. Resonant excitation of a core level electron into unoccupied states of the conduction band (CB) (Equation S3);

*IV. After process III, an electron from the VB refills the core hole transferring the energy to the initial excited core level electron thus exciting it above **E**$_{Vac}$ (participator decay), (Equation S4);*

V. After process II, an electron from the VB refills the core hole with the emission of a photon (Equation S5).

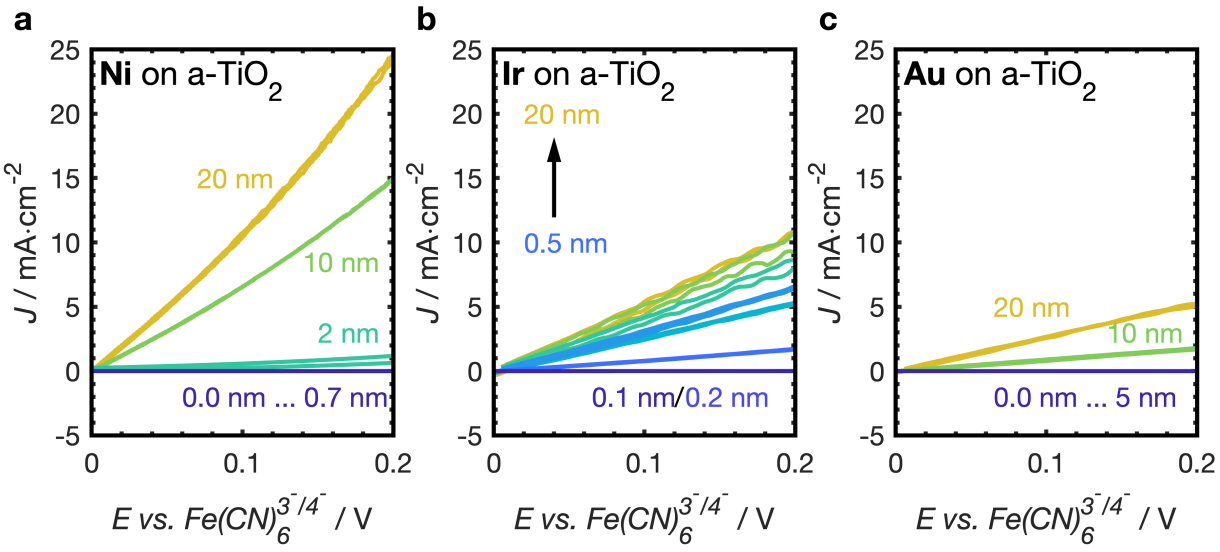

Figure S2: *J-E measurements for* ***(a)*** *p^+-Si/a-TiO_2/Ni,* ***(b)*** *p^+-Si/a-TiO_2/Ir, and* ***(c)*** *p^+-Si/a-TiO_2/Au in 0.05/0.35 M $Fe(CN)_6^{3-/4-}$(aq) with different thicknesses of the metal layer.*

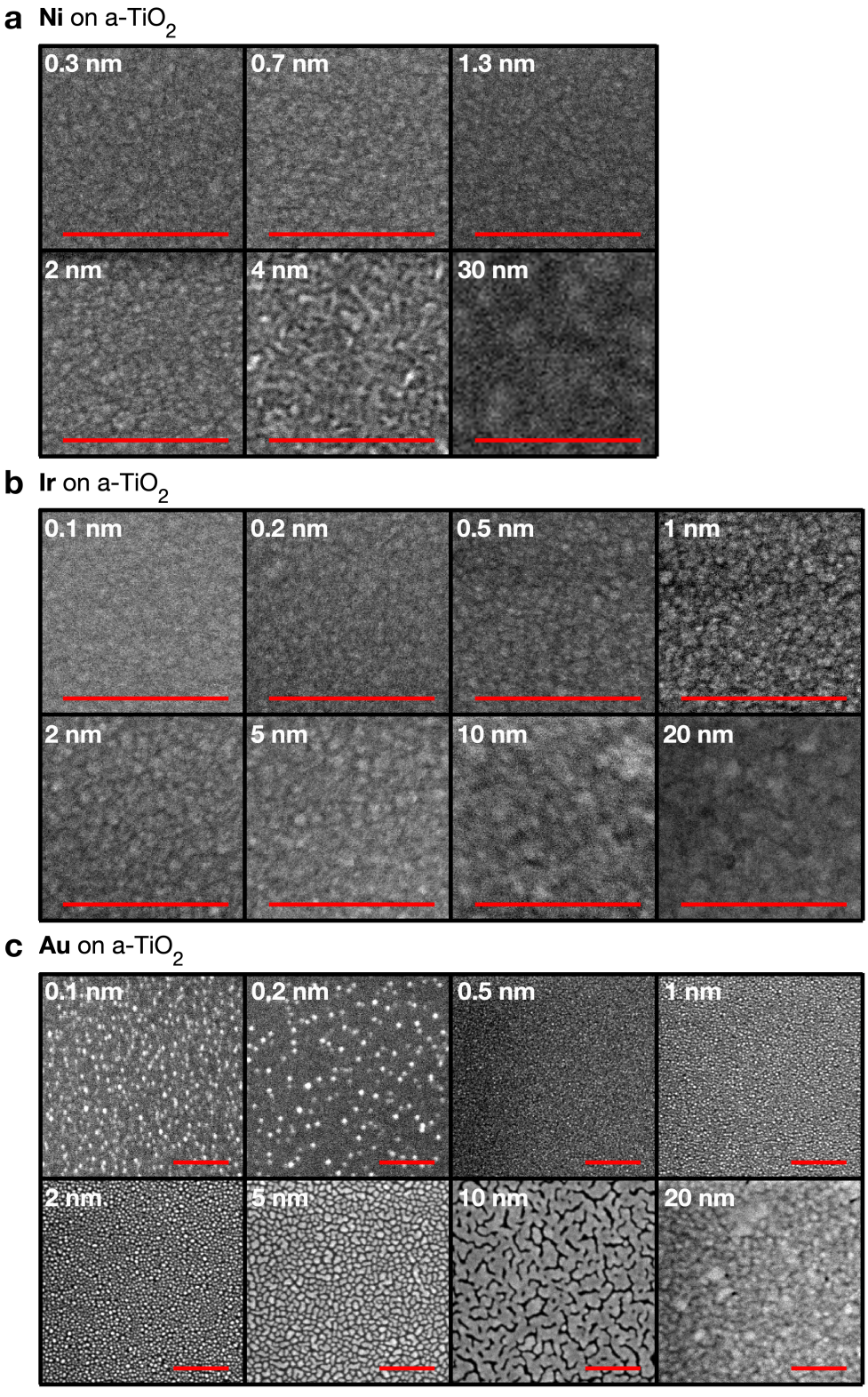

Figure S3: *Scanning-electron microscopy images of a-TiO_2/M: M = Ni* ***(a)****, Ir* ***(b)****, and Au* ***(c)*** *for different metal thicknesses. The scale bar is 200 nm.*

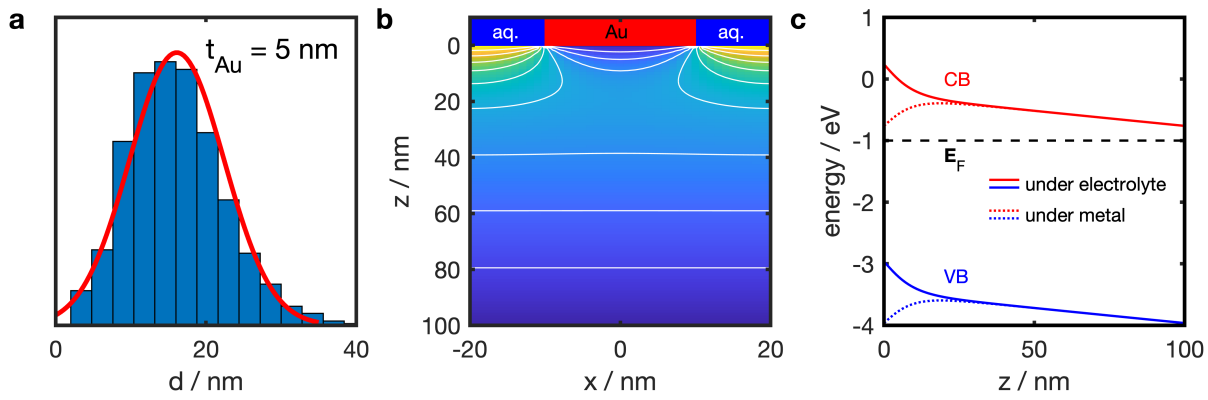

Figure S4: ***(a)*** *Gold nanoparticle size distribution for nominal Au thicknesses of 5 nm on a-TiO_2 (Figure S3c).* ***(b)*** *Potential distribution for a 20 nm Au nanoparticle on a-TiO_2 under +1 V bias calculated using the full Poisson equation with Fermi-Dirac statistics for a free charge-carrier concentration in a-TiO_2 of 1×10^{16} cm^{-3} with periodic boundary conditions* [2]. ***(c)*** *Band diagram for a 20 nm Au nanoparticle on a-TiO_2 under +1 V bias. Solid line shows the band alignment of a-TiO_2 under the bulk electrolyte, whereas the dotted line indicated the band alignment directly under the Au nanoparticle. A barrier for hole transport to the gold particle is visible.*

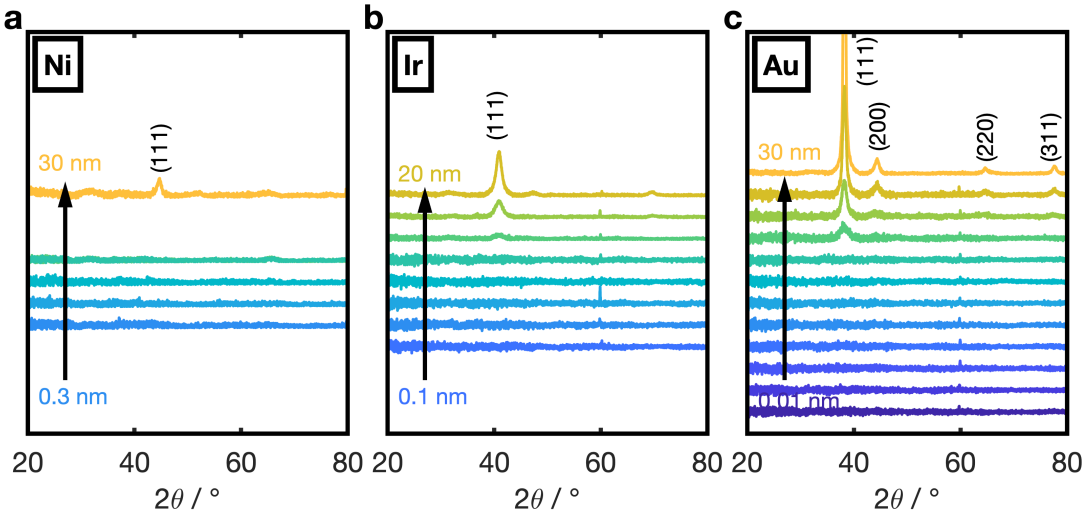

Figure S5: *XRD spectra for a-TiO_2/M (M=Ni, Ir, Au) for different metal layer thicknesses. The nominal metal layer thicknesses are 0.3, 0.7, 1, 2 and 30 nm for Ni ;0.1, 0.2, 0,5, 1, 2, 5, 10 and 20 nm for Ir; 0.01, 0.02, 0.05, 0.1, 0.2, 0.5, 1, 2, 5, 10, 20 and 30 nm for Au.*

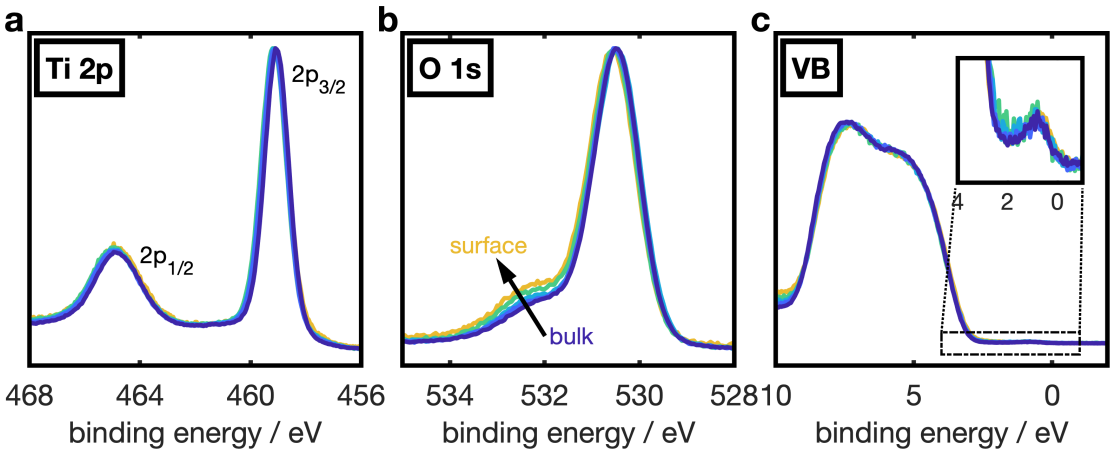

Figure S6: *XPS data for TDMAT ALD a-TiO_2 of the Ti 2p* ***(a)*** *and O 1s* ***(b)*** *core levels and of the VB* ***(c)*** *for different photoelectron emission angles from θ = 0° (bulk sensitive) to θ = 70° (surface sensitive) relative to the surface normal. With increased surface sensitivity (increased θ), an increase in the oxygen shoulder at 532.5 eV was observed.*

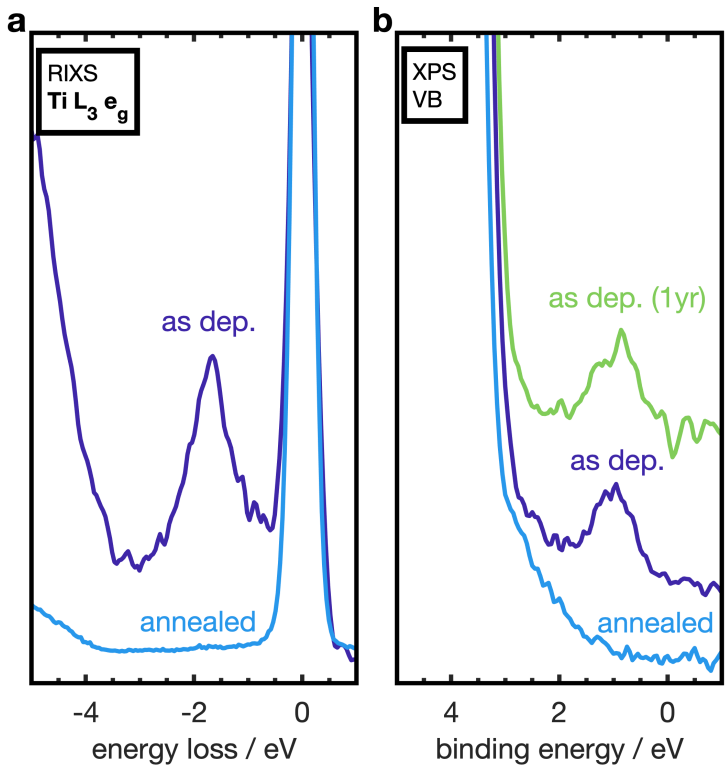

Figure S7: ***(a)*** *RiXS data at the Ti L_3 e_g resonance for as deposited (as dep.) TiO_2 and* ***(b)*** *XPS VB data for TiO_2 annealed in air (450 °C for 1 h), as deposited (as dep.), and after storing in air for 1 year (as dep. (1 yr)), respectively. The gap state seen at 1 eV binding energy below the Fermi level is observed at and energy loss of 1.8 eV below the CBM in the RiXS spectra.*

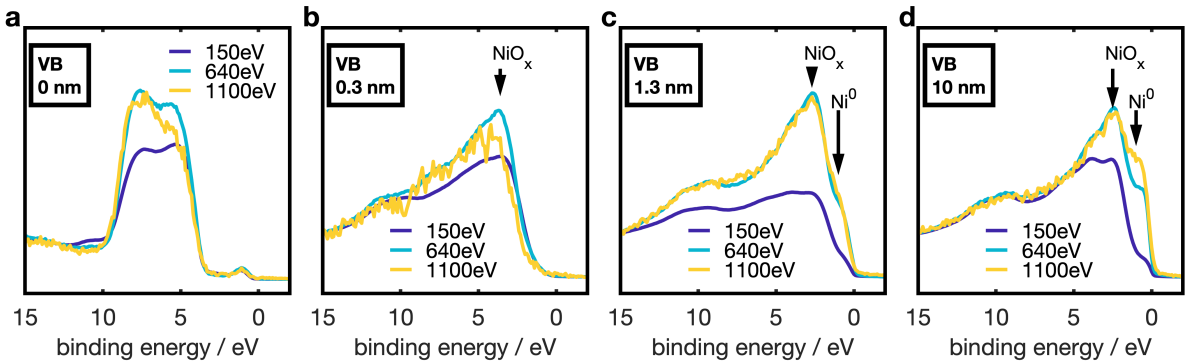

Figure S8: *VB spectra of for different nickel thicknesses:* ***(a)*** *0 nm,* ***(b)*** *0.3 nm,* ***(c)*** *1.3 nm and* ***(d)*** *10 nm. The spectra were recorded at three different photon energies: 150 eV, 640 eV and 1100 eV corresponding also to the kinetic energy of electron from the upper VB. Hence, the inelastic mean-free path (IMFP) of the photoelectrons corresponds to* λ *= 4.72 Å (Ni) to 6.28 Å (a-*TiO_2*) for* $\boldsymbol{E}_K$ *= 150 eV,* λ *= 11.19 Å (Ni) to 14.96 Å (a-*TiO_2*) for* $\boldsymbol{E}_K$ *= 640 eV and* λ *= 16.64 Å (Ni) to 22.39 Å (a-*TiO_2*) for* $\boldsymbol{E}_K$ *= 1100 eV. Values for the Inelastic Mean-Free Path for elements under investigation for relevant photoelectron energies were calculated using IMFP-TPP2M.* [3]

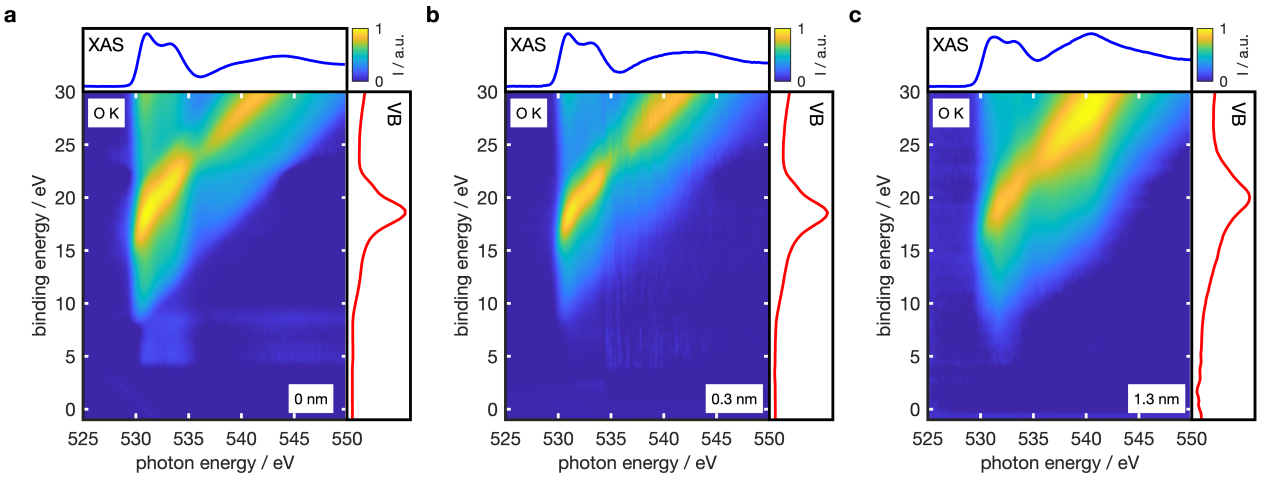

Figure S9: *Resonant photoemission maps at the Oxygen K edge of* ***(a)*** *p^+-Si/a-TiO_2,* ***(b)*** *p^+-Si/a-TiO_2/Ni(0.3 nm) and* ***(c)*** *p^+-Si/a-TiO_2/Ni(1.3 nm). The insets on the top show the TEY XAS spectrum and the insets on the right show the VB spectrum at 531 eV. In all spectra, the off-resonant contributions were subtracted using the off-resonant VB spectra at 525 eV. Above 9 eV, the spectra at higher binding energies are dominated by the spectator Auger process.*

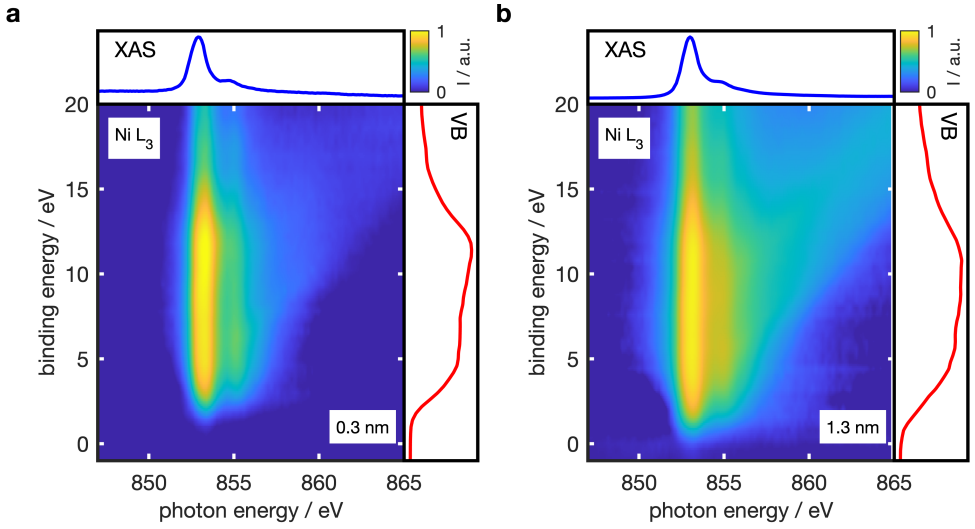

Figure S10: *Resonant photoemission maps at the Ni L_3 edge of* ***(a)*** *p^+-Si/a-TiO_2/Ni(0.3 nm) and* ***(b)*** *p^+-Si/a-TiO_2/Ni(1.3 nm). The insets on the top show the TEY XAS spectrum and the insets on the right show the VB spectrum at 853 eV. In all spectra, the off-resonant contributions were subtracted using the off-resonant VB spectra at 846 eV.*

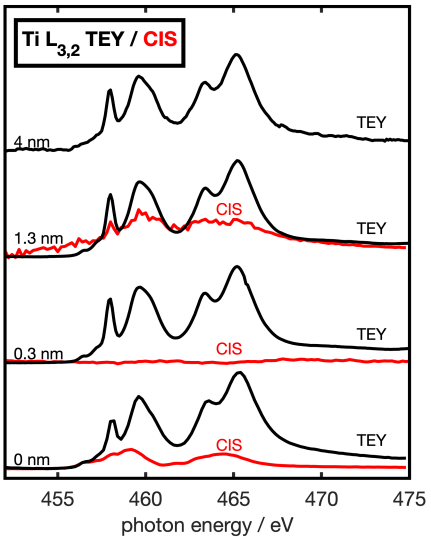

Figure S11: *Total electron yield (TEY) mode XAS spectrum (black line) and constant initial state (CIS) XAS spectrum (red line) integrated over the binding energy range of the gap state(s) (0 - 3 eV) for various thickness of Ni. The TEY-XAS shows almost no change with Ni suggesting the majority a-TiO_2 would not change while the CIS-XAS shows additional intensity at lower photon energy (< 457 eV) which may suggest some reduction of the TiO_2.* [4,5]

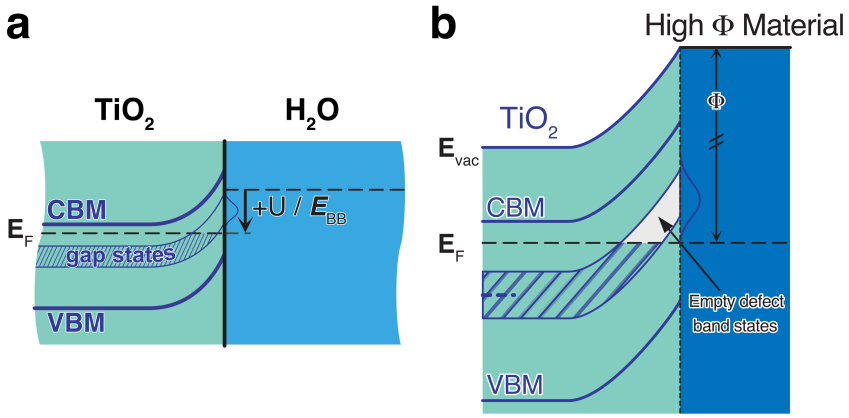

Figure S12: ***(a)*** *Band diagram of a-TiO_2 in contact with electrolyte under positive bias (negative* $\boldsymbol{E_{BB}}$*). For increased positive potentials (negative* $\boldsymbol{E_{BB}}$*) the Fermi level crosses the gap states.* [6] ***(b)*** *Band diagram of a-TiO_2 in contact with a high work-function material. Upward band bending above Fermi level leads to empty defect band states with a reduced* Ti^{3+} *concentration. If hole transport proceeds via a hopping process* $Ti^{3+} + Ti^{4+} \rightarrow Ti^{4+} + Ti^{3+}$*, the rate of this second order reaction is proportional to the concentrations of both* Ti^{3+} *and* Ti^{4+}*. The total number of* Ti *sites are fixed, so the rate is maximized when the concentrations are equal* $[Ti^{3+}] = [Ti^{4+}]$*. The reduced* Ti^{3+} *would therefore substantially decrease the rate of transfer and consequently the conduction current.*

Table S1: *Parameters used for band-energy diagrams of a-TiO_2/M with M=nickel, M=iridium and M=gold as shown in Figure 7.* $\boldsymbol{E_{BB}}$ *is the band bending at the interface. The band gap for a-TiO_2 was taken from previous studies.* [7,8]

	a-TiO_2/Ni	**a-TiO_2/Ir**	**a-TiO_2/Au**
Φ(a-TiO_2) / eV	4.70	4.70	4.70
Φ(M) / eV	5.09	5.32	5.05
$\boldsymbol{E}_g$(a-TiO_2) / eV	3.34	3.34	3.34
$\boldsymbol{E}_B$(Ti 2p, bulk)	459.25	459.25	459.25
$\boldsymbol{E}_B$(M, bulk) / eV	852.6	60.9	84
$\boldsymbol{E}_{BB}$(a-TiO_2) / eV	-0.19	-0.92	-0.05
δ (dipole) / eV	0.20	-0.30	0.30
$\boldsymbol{E}_B$(gap state, bulk)	1.0	1.0	1.0
FWHM(gap state, bulk) / eV	0.88	0.88	0.88
$\boldsymbol{E}_B$(gap state, interface) /eV	0.7, 2.6	0.08	0.95
FWHM(gap state, interface) / eV	1.4, 1.2	0.88	0.88

References

1. Stöhr, J. *NEXAFS Spectroscopy,* 2nd ed.; Springer: Heidelberg, 2003; Vol. 25.
2. Nunez, P.; Richter, M. H.; Piercy, B. D.; Roske, W. C.; Cabań-Acevedo, M.; Losego, M. D.; Konezny, S. J.; Fermin, D. J.; Hu, S.; Brunschwig, B. S.; Lewis, N. S. Characterization of Electronic Transport through Amorphous TiO_2 Produced by Atomic Layer Deposition. *J. Phys. Chem. C* **2019,** *123* (33), 20116-20129.
3. Tanuma, S.; Powell, C. J.; Penn, D. R. Calculations of Electron Inelastic Mean Free Paths. V. Data for 14 Organic Compounds Over the 50–2000 eV Range. *Surf. Interface Anal.* **1993,** *21* (3), 165-176.
4. Rotundu, C. R.; Jiang, S.; Deng, X.; Qian, Y.; Khan, S.; Hawthorn, D. G.; Kotliar, G.; Ni, N. Physical Properties and Electronic Structure of a New Barium Titanate Suboxide $Ba_{1+\delta}Ti_{13-\delta}O_{12}$ ($\delta = 0.11$). *APL Materials* **2015,** *3* (4), 041517.
5. Singh, R.; Gupta, M.; Phase, D. M.; Mukherjee, S. K. Phase Growth Analysis of Sputtered TiO_2 Thin Films at Low Oxygen Partial Pressures Using XANES and XRR. *Mater. Res. Express* **2019,** *6* (11), 116449.
6. Lichterman, M. F.; Richter, M. H.; Hu, S.; Crumlin, E. J.; Axnanda, S.; Favaro, M.; Drisdell, W.; Hussain, Z.; Brunschwig, B. S.; Lewis, N. S.; Liu, Z.; Lewerenz, H. J. An Electrochemical, Microtopographical and Ambient Pressure X-Ray Photoelectron Spectroscopic Investigation of Si/TiO_2/Ni/Electrolyte Interfaces. *J. Electrochem. Soc.* **2015,** *163* (2), H139-H146.
7. Hu, S.; Shaner, M. R.; Beardslee, J. A.; Lichterman, M.; Brunschwig, B. S.; Lewis, N. S. Amorphous TiO_2 Coatings Stabilize Si, GaAs, and GaP Photoanodes for Efficient Water Oxidation. *Science* **2014,** *344* (6), 1005-1009.
8. Hu, S.; Richter, M. H.; Lichterman, M. F.; Beardslee, J.; Mayer, T.; Brunschwig, B. S.; Lewis, N. S. Electrical, Photoelectrochemical, and Photoelectron Spectroscopic Investigation of the Interfacial Transport and Energetics of Amorphous TiO_2/Si Heterojunctions. *J. Phys. Chem. C* **2016,** *120* (6), 3117-3129.